Sensors and Actuators A 215 (2014) 150–154

Contents lists available at ScienceDirect

Sensors and Actuators A: Physical

journal homepage: www.elsevier.com/locate/sna

Electrostatic and mechanical characterization of 3-D micro-wineglass resonators

D. Senkal*, M.J. Ahamed, A.A. Trusov, A.M. Shkel

MicroSystems Laboratory, 4200 Engineering Gateway Building, Department of Mechanical and Aerospace Engineering, University of California, Irvine, CA 92697, United States

ARTICLE INFO

Article history:
Received 28 May 2013
Received in revised form 17 January 2014
Accepted 3 February 2014
Available online 18 February 2014

Keywords:
Micro-glassblowing
3-D MEMS
Adjustable electrodes
MEMS ratchet mechanism
Wineglass resonator

ABSTRACT

In this paper, we present methods for characterization of 3-D micro-wineglass resonators. Two interchangeable modes of excitation are demonstrated: (1) Mechanical pinging using a piezo actuated probe assembly and (2) electrostatic excitation using assembled electrode structures. Two interchangeable modes of detection are also presented: optical pick-up using laser Doppler vibrometry and capacitive detection. 3-D micro-glassblown wineglass resonators were used to demonstrate the characterization methods in this paper. Electrostatic excitation was used to obtain the frequency response of micro-glassblown resonators showing a Q-factor of 40.000 at 14.8 kHz, whereas piezo-pinging was used to obtain the time domain response of the resonators.

1. Introduction

There is a growing interest in 3-D MEMS wineglass resonators for the next generation timing, signal processing, and inertial sensing applications due to potential advantages of the wineglass geometry in terms of symmetry, minimization of energy loss, thermal stability, and immunity to external vibrations [1]. However, difficulties associated with fabricating smooth, symmetric, high aspect ratio 3-D structures have so far prevented their integration with MEMS techniques.

With the emergence of new 3-D micro-machining techniques, batch fabrication of 3-D MEMS wineglass structures is becoming feasible. For instance, hemispherical shells fabricated by deposition of polysilicon [2], poly-crystalline diamond [3] or silicon nitride [4] thin films into isotropically etched cavities have recently been demonstrated. Alternative fabrication techniques include thin film deposition onto high-precision ball bearings [5], "3-D SOULE" (micro ultrasonic machining, lapping, and micro electro-discharge machining) process for fabrication of mushroom and concave shaped spherical structures [6], as well as the pressure/surface tension driven fabrication techniques such as blow molding of bulk metallic glasses into pre-etched cavities [7], blow-torch molding of fused silica shells [8] and micro-glassblowing of borosilicate glass [9–13] or fused silica [8,14,15] into spherical or wineglass geometries.

Despite the recent advances in micro-wineglass resonator fabrication, the technology development is in its infancy and characterization of the early stage prototypes presents a challenge. This paper introduces interchangeable excitation and detection methods for characterization of micro-wineglass devices of any shape or size, eliminating the need for in situ electrode fabrication during the development cycle of the resonator architecture, Fig. 1. Additionally, mechanical excitation capability eliminates the need for conductive coating of dielectric resonators, electrical feed-throughs or DC biasing, all of which can obscure the actual resonator performance.

Two interchangeable modes of excitation are presented: Mechanical pinging and electrostatic excitation, Fig. 2 [16]. Mechanical pinging is provided by a piezo actuated probe assembly, whereas electrostatic excitation is provided by assembled electrode structures with <20 μm capacitive gaps. Two modes of detection are also available: optical pick-up and capacitive detection, Fig. 2. Optical pick-up is provided by laser Doppler vibrometry (LDV) and capacitive detection is provided by assembled electrode structures. 3D micro-glassblown wineglass resonators were used to demonstrate the capabilities of the test-bed in extracting resonator parameters such as Q-factor or frequency split between degenerate wineglass modes.

In the following sections, we will first present the micro-wineglass resonator fabrication process. This will be followed by

* Corresponding author. Tel.: +1 949 945 0858.
E-mail addresses: dsenkal@uci.edu, doruksenkal@gmail.com (D. Senkal).

http://dx.doi.org/10.1016/j.sna.2014.02.001
0924-4247/

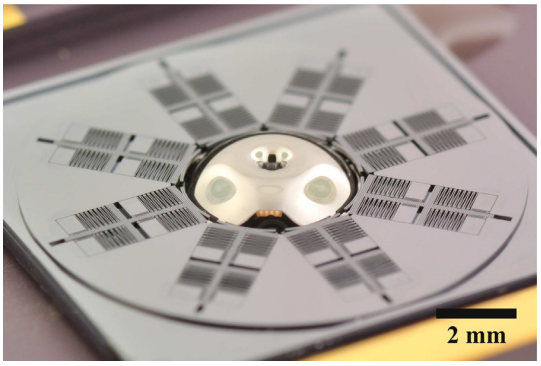

Fig. 1. Electrode structures assembled onto a micro-glassblown wineglass resonator with <20 μm gaps.

the design and operation of the assembled electrode structures and the piezo-pinger setup. The paper concludes with a comparative analysis of the two testing methods.

2. Fabrication of wineglass structures

Micro-wineglass resonators presented in this paper were fabricated using a micro-glassblowing process, Fig 3. This process utilizes an etched cavity on a substrate wafer and a glass layer that is bonded on top of this cavity, creating a volume of trapped gas for subsequent glassblowing of self-inflating shells. When the bonded wafer stack is heated above the softening point of the structural glass layer, two effects are activated at the same time: (1) the glass layer becomes viscous, and (2) the air pressure inside the pre-etched cavity raises above the atmospheric level. This results in plastic deformation of the glass layer, driven by gas pressure and surface tension forces (glass-blowing). The expansion of air (and hence the formation of the shell) stops when the pressure inside and outside of the glass shell reaches an equilibrium. During this deformation, the surface tension acting on the (now viscous) glass layer works toward minimizing the surface area of the structure, as a result a highly symmetric shell with low surface roughness forms, Fig. 4.

In order to fabricate the micro-wineglass resonators, first cylindrical cavities with a central post are etched to a 250 μm depth on a silicon substrate wafer using DRIE, Fig. 3. This is followed but bonding of the glass layer (100 μm) onto the silicon substrate. The glass layer bonds to the substrate along the perimeter of the cylindrical cavity and at the central post. Then the outer perimeter of the wineglass resonator and the central via hole Fig. 3(b) is defined using glass dry etching. The glass etching is performed using a magnetic neutral loop discharge plasma oxide etcher (ULVAC NLD 570 Oxide Etcher) [17]. A low-stress electroplated Cr/Ni hard-mask was used to etch the 100 μm deep trenches. This is followed by micro-glassblowing of the wafer stack at 875 °C inside a RTA system, where the glass layer becomes viscous and the air inside the

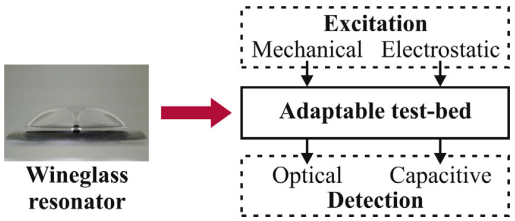

Fig. 2. Schematic description of adaptable test-bed for characterization of micro-wineglass prototypes.

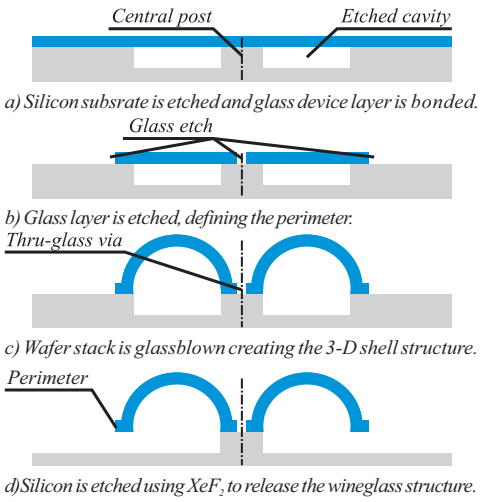

Fig. 3. Micro-glassblown wineglass structures are fabricated by (a) etching cavities on the substrate layer, (b) etching of the glass layer to define the perimeter, (c) micro-glassblowing above the softening point of the glass layer and (d) etching away the substrate underneath the wineglass structure.

cavity expands, creating the 3-D shell structure seen in Fig. 3(c). A self-aligned central stem structure is also formed at this step due to the deformation of the glass layer around the central anchor point. The perimeter of the wineglass structure does not deform as there is no etched cavity under these structures, enabling lithographic definition of the perimeter of the wineglass. The next step is XeF_2 etching of the substrate underneath the glass layer in order to release the wineglass resonator along its perimeter, Fig. 3(d). XeF_2 is chosen because of the extremely high selectivity to glass (as high as 1:1000 selectivity). Once the etch is complete a free standing micro-wineglass structure with a self-alinged stem structure is obtained, Fig. 4. Final step of the fabrication process is blanket metallization by sputtering or atomic layer deposition (ALD), Fig. 3(e). A monolayer of Iridium was chosen for the metal layer seen in Fig. 3, because of high conductivity, corrosion resistance and the ability to apply without utilizing an adhesion layer. The metal layer coats the top surface of the resonator shell, the side walls of the capacitive gaps as well as inside of the central via hole. Electrical feed-through to the resonator is obtained through the central via structure, which connects the resonator onto the substrate.

3. Assembled electrodes

Electrostatic excitation and detection is provided by assembled electrode structures, which are fabricated separately from the

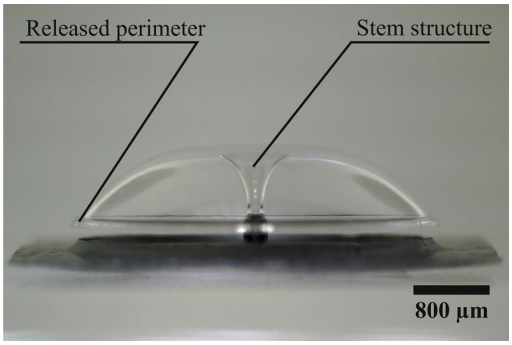

Fig. 4. Released wineglass structure with 4.2 mm diameter, 50 μm thickness and 300 μm central stem.

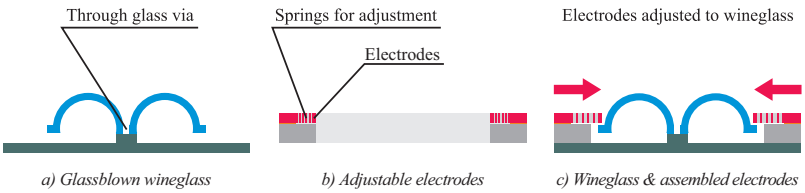

Fig. 5. Electrodes are fabricated separately on an SOI stack, bonded onto the resonator wafer and adjusted to the resonator.

micro-glassblown resonator on a SOI wafer, Fig. 5. The SOI stack consists of 500 μm silicon substrate layer, 5 μm buried oxide layer and 100 μm silicon device layer. Each electrode assembly consists of 8 independent electrodes that are spaced 45 apart around a central thru-hole. Large spring structures on each electrode allow an adjustment distance up to 400 μm for each individual electrode (total of 800 μm along the resonator diameter), which permits a single electrode design to be used for different wineglass architectures and diameters, Fig. 6. Electrode assemblies with 7 different central-hole diameters were fabricated on the same SOI wafer, which covers all wineglass diameters from 1 mm to 4.5 mm.

The fabrication of SOI electrodes start by lithographically patterning the back-side thru-hole and etching using DRIE to a depth of 500 μm. This is followed by patterning and etching the device layer to create the electrode structures. For the electrode structures, the DRIE is performed to a depth of 100 μm, using a 1.6 μm oxide hard-mask for better feature resolution, then O_2 ashing/RCA-1 cleaning is used to get rid of excess photoresist and etch residues. The final step of the fabrication process is HF wet etching of buried oxide layer to release the electrode structures.

3.1. Operation

Once the fabrication is complete the electrode structures are singulated and bonded onto the micro-wineglass die, Fig. 5. Then, each electrode is pushed to close proximity of the wineglass by using a micro-manipulator. When the correct location is achieved four ratchet mechanisms (2 front, 2 back) keep the electrodes in place, Fig. 7. The ratchet mechanisms act on 2 rack gears placed on the electrode. The pitch distance on the rack gears are 20 μm. By offsetting the front and rear ratchet mechanisms by 10 μm relative to the teeth pitch of the rack gear, a positioning resolution of 10 μm was obtained (minimum capacitive gap).

For experimental characterization, assembled electrodes were bonded onto micro-glassblown wineglass structures, Fig. 4. A wineglass with 4.2 mm diameter, 50 μm thickness, and 300 μm central stem was tested using an assembled electrode structure with

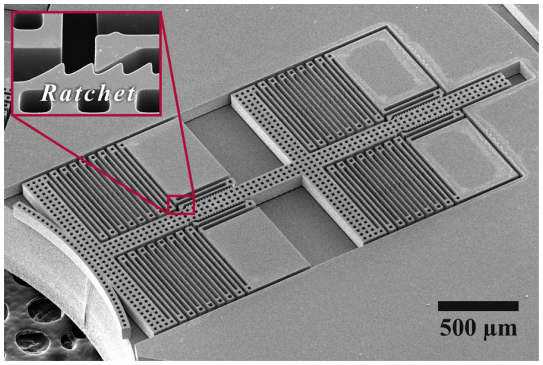

Fig. 6. SEM image of an adjustable electrode with 400 μm maximum displacement and 10 μm positioning resolution.

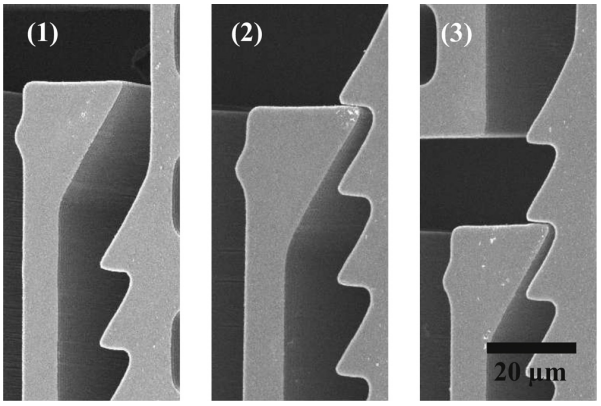

Fig. 7. Ratchet mechanism acting on the electrode structure, the electrode is extended gradually in 1 through 3.

4.5 mm thru-hole. The entire assembly was placed into a ceramic DIP package with gold back-plate and wirebonded at the anchors of each electrode. The bias voltage to the resonator is applied through the gold back-plate, which connects to the resonator die, through it to the via at the center of the stem and to the resonator metal layer.

Frequency sweeps were obtained using an Agilent 4395A network analyzer. Two opposite electrodes were used with the goal of forced excitation of the $n=2$ wineglass mode. A DC voltage of 10 V and AC voltage of 5 V_{pp} were used. A Q-factor of 40.000 was observed at 14.833 kHz, giving a time decay constant of 0.9 s, Fig. 8.

Adjustable nature of the assembled electrode structures allow, characterization of 3-D resonator structures with varying size and diameter. Fig. 9 shows assembled electrodes structures around a 1.2 mm micro-glassblown spherical resonator with resonant frequencies in the MHz range.

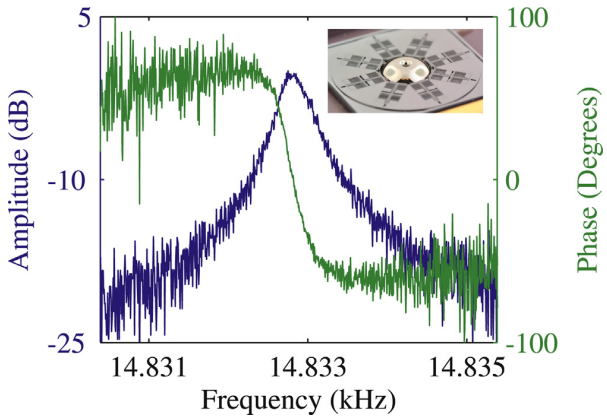

Fig. 8. Electrostatic frequency sweep, using adjustable electrode assembly, showing $Q=40k$ at 14.8 kHz.

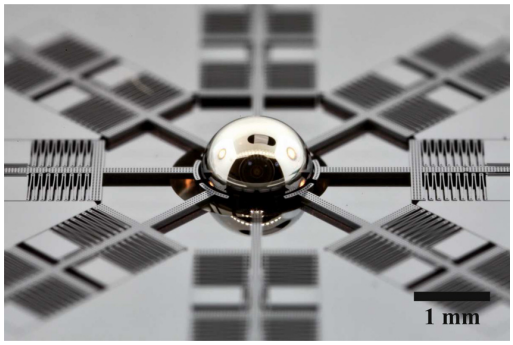

Fig. 9. A glassblown spherical resonator with assembled electrodes. Diameter is 1.2 mm and thickness is ~5 μm.

4. Piezo-pinger setup

Capacitive transduction requires an electrical connection to the resonator body, which can be achieved either by using a conductive resonator material or coating the resonator with a conductive layer. If the resonator is made out of a dielectric material, such as SiO_2, conductive coating with an appropriate feed-through might not be available during early stages of the resonator fabrication. Otherwise, it might be undesirable to use capacitive transduction for testing, since factors such as electrostatic coupling effect or metallization losses can obscure the actual mechanical characteristics of the wineglass resonator. For these reasons a mechanical excitation method that can operate under vacuum and directionally excite the wineglass modes is highly desirable as an alternative to electrostatic transduction.

A piezo-pinger setup was constructed using off-the-shelf components and rapid prototyped fixtures. The piezo-pinger assembly consists of 3 main components: A linear micro-stage with a positioning accuracy of 1 μm, a high displacement (32 μm) piezo-stack, and a tungsten probe tip (100 μm tip radius), Fig. 10. The setup is built with vacuum compatible components and fits into a bounding box of 80 mm × 30 mm × 20 mm.

4.1. Operation

Wineglass resonator is placed on the linear stage and kept in place using a non-permenant bonding method, such as indium or double sided kapton tape. Linear stage is adjusted under a microscope until the probe tip is within 5–10 μm proximity of the wineglass. Then, the piezo-pinger is placed into the vacuum chamber and connected to a high-voltage power supply 12. A mechanical

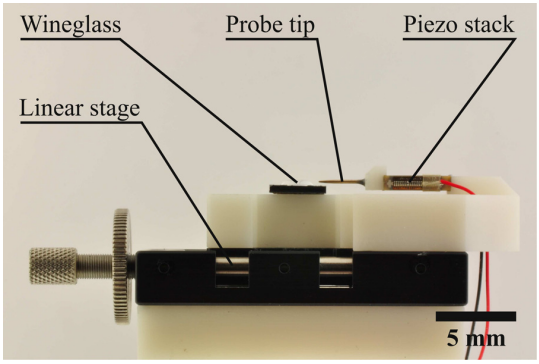

Fig. 10. Piezo-pinger setup for time domain characterization, piezo stack is actuated to probe the wineglass resonator.

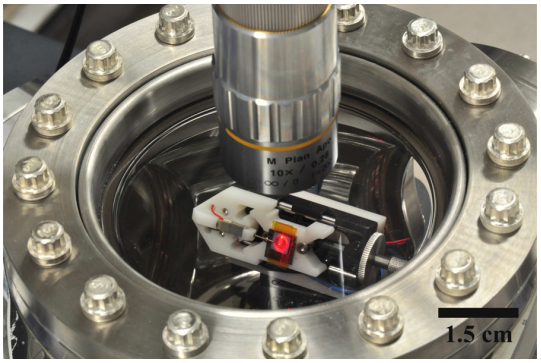

Fig. 11. Piezo-pinger setup inside vacuum chamber. Optical port on the vacuum chamber allows laser Doppler vibrometer characterization.

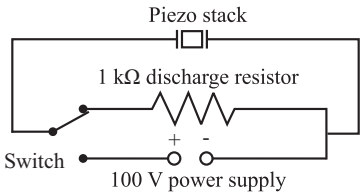

Fig. 12. A mechanical switch with 1 kΩ discharge resistor was used for controlling the piezo-stack.

switch with 1 kΩ discharge resistor was used for controlling the piezo-stack, Fig. 11. A Polytec laser Doppler vibrometer pointed onto the outer edge of the wineglass resonator through the optical port of the vacuum chamber is used for detection, Fig. 11.

Experiment starts by increasing the voltage on the piezo-stack until the probe tip barely makes contact with the edge of the wineglass (up to 100 V DC), which applies a point load onto the wineglass resonator. At the beginning of the experiment the probe tip is retracted by shorting the piezo-stack over the 1 kΩ discharge resistor, Fig. 12. A short period (1–5 ms) of transient behavior is observed, where the shell undergoes a large deformation due to the interaction with the piezo pinger. After this transient, which saturates the laser Doppler vibrometer (LDV), free vibration of the shell structure starts ($t = 0$). Time domain response is captured using the laser Doppler vibrometer at a sampling rate of 1256 kHz. The data can later be analyzed either in the time domain or in frequency domain using a Fast Fourier Transform (FFT) algorithm.

Time domain response, in Fig. 13, was obtained on a wineglass resonator using the described piezo-pinger setup and laser

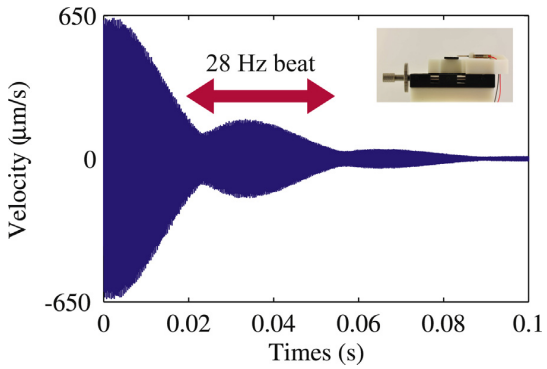

Fig. 13. Time decay response obtained by retracting the probe tip, beat signal between two degenerate modes shows $\Delta f = 28$ Hz.

Table 1
Comparison of excitation methods.

	Assembled electrodes	Piezo-pinger
Attachment	Permanent	Non-permanent
Coating	Metalized	None required
Detection	Electrostatic	Laser vibrometer
Mode selection	Yes	No

Doppler vibrometer detection. Fig. 13 shows a 28 Hz beat signal created by the frequency split between two degenerate wineglass modes. Post-processing using a FFT algorithm confirms the frequency split of 28 Hz at resonant frequencies $f_1 = 22036$ Hz and $f_2 = 22064$ Hz. Large frequency split is associated primarily with dry etch defects at around the perimeter of the wineglass, followed by the influence of g-forces and thermal non-uniformities within the micro-glassblowing furnace. These effects have been addressed recently [17] to achieve sub-Hz frequency symmetry in micro-glassblown wineglass resonators [18].

5. Comparison of excitation methods

A comparative summary of the two excitation methods is presented in Table 1. Assembled electrode structures are more suited for detailed characterization of wineglasses due to the capability of mode selection and continuous excitation at the cost of potentially unwanted need for metallization and permanent attachment to the shell. Whereas, piezo-pinger setup is ideal for rapid characterization of wineglasses as it does not require permanent attachment or metallization.

Another advantage of the piezo-pinger setup is the fact that metallization of the shells is not required for characterization. This way unwanted metallization losses can be eliminated, which could potentially obscure the actual resonator behavior. Even though no significant Q-factor change has been observed on borosilicate glass shells, metallization losses are expected to play a role in higher Q-factor fused silica and ULE TSG shells.

6. Conclusions

Micro-wineglass resonators were fabricated through micro-glassblowing process. Micro-wineglass structures were released on wafer-scale through deep glass dry etching and XeF_2 etching. The fabricated micro-wineglass resonators were tested electrostatically and mechanically using assembled-electrode structures and piezo-pinger setup.

Electrostatic excitation has advantages in terms of mode selectivity as unwanted modes can be suppressed by using a combination of balanced electrodes. However, it can potentially obscure the actual resonator behavior due to metallization losses or the electrostatic coupling effect. Both of these effects can be avoided by using a purely mechanical excitation method, such as piezo-pinging. Another benefit of the piezo-pinger setup is the non-permanent attachment of the resonator, which allows quick testing of multiple wineglass resonators.

By decoupling the resonator development from electrode fabrication, a greater flexibility in design and fabrication is obtained. In addition, the methods presented in this paper is universally applicable to any micro-wineglass resonator, regardless of shape, size or fabrication process involved.

Acknowledgements

This material is based upon work supported by DARPA grant W31P4Q-11-1-0006 (Program Manager Dr. Robert Lutwak). Devices were designed and tested in UCI MicroSystems Lab. Authors would like to thank UCI INRF staff Jake Hes, Mo Kebaili, Vu Phan and Lifeng Zheng for their help and valuable suggestions on the fabrication aspects of the project.

References

[1] D.M. Rozelle, The hemispherical resonator gyro: from wineglass to the planets, in: Proceedings of AAS/AIAA Space Flight Mechanics Meeting, 2009, pp. 1157–1178.
[2] L.D. Sorenson, X. Gao, F. Ayazi, 3-D micromachined hemispherical shell resonators with integrated capacitive transducers, in: IEEE MEMS, 2012, pp. 168–171.
[3] M.L. Chan, J. Xie, P. Fonda, H. Najar, K. Yamazaki, L. Lin, D.A. Horsley, Micromachined polycrystalline diamond hemispherical shell resonators, in: Solid-State Sensors, Actuators, and Microsystems Workshop (Hilton Head), Hilton Head Island, SC, USA, 2012, pp. 355–358.
[4] L.C. Fegely, D.N. Hutchison, S.A. Bhave, Isotropic etching of 111 SCS for wafer-scale manufacturing of perfectly hemispherical silicon molds, in: Solid-State Sensors, Actuators, and Microsystems Workshop (TRANSDUCERS), Beijing, China, 2011, pp. 2295–2298.
[5] Y. Xie, H.C. Hsieh, P. Pai, H. Kim, M. Tabib-Azar, C.H. Mastrangelo, Precision curved micro hemispherical resonator shells fabricated by poached-egg micromolding, in: IEEE Sensors, 2012, pp. 279–283.
[6] K. Visvanathan, T. Li, Y. Gianchandani, 3D-soule: a fabrication process for large scale integration and micromachining of spherical structures, in: IEEE MEMS, 2011, pp. 45–48.
[7] B. Sarac, G. Kumar, T. Hodges, S. Ding, A. Desai, J. Schroers, Three-dimensional shell fabrication using blow molding of bulk metallic glass, Journal of Microelectromechanical Systems 20 (1) (2011) 28–36.
[8] J. Cho, J. Yan, J.A. Gregory, H. Eberhart, R.L. Peterson, K. Najafi, High-q fused silica birdbath and hemispherical 3-d resonators made by blow torch molding, in: IEEE MEMS, Taipei, Taiwan, 2013, pp. 177–180.
[9] E.J. Eklund, A.M. Shkel, Self-inflated micro-glass blowing, US Patent 8,151,600.
[10] E.J. Eklund, A.M. Shkel, Glass blowing on a wafer level, Journal of Microelectromechanical Systems 16 (2) (2007) 232–239.
[11] D. Senkal, I.P. Prikhodko, A.A. Trusov, A.M. Shkel, Micromachined 3-D glass-blown wineglass structures for vibratory MEMS applications, in: Technologies for Future Micro-Nano Manufacturing Workshop, Napa, CA, USA, 2011, pp. 166–169.
[12] I.P. Prikhodko, S.A. Zotov, A.A. Trusov, A.M. Shkel, Microscale glass-blown three-dimensional spherical shell resonators, Journal of Microelectromechanical Systems 20 (3) (2011) 691–701.
[13] S.A. Zotov, I.P. Prikhodko, A.A. Trusov, A.M. Shkel, 3-D micromachined spherical shell resonators with integrated electromagnetic and electrostatic transducers, in: Solid-State Sensors, Actuators, and Microsystems Workshop (Hilton Head), Hilton Head Island, SC, USA, 2010, pp. 11–14.
[14] D. Senkal, C.R. Raum, A.A. Trusov, A.M. Shkel, Titania silicate/fused quartz glass-blowing for 3-D fabrication of low internal loss wineglass micro-structures, in: Solid-State Sensors, Actuators, and Microsystems Workshop (Hilton Head), Hilton Head Island, SC, USA, 2012, pp. 267–270.
[15] D. Senkal, M.J. Ahamed, A.A. Trusov, A.M. Shkel, High temperature micro-glassblowing process demonstrated on fused quartz and ULE TSG, Sensors and Actuators A: Physical 201 (2012) 525–531.
[16] D. Senkal, M.J. Ahamed, A.A. Trusov, A.M. Shkel, Adaptable test-bed for characterization of micro-wineglass resonators, in: IEEE MEMS, Taipei, Taiwan, 2013, pp. 469–472.
[17] M.J. Ahamed, D. Senkal, A.A. Trusov, A.M. Shkel, Deep NLD plasma etching of fused silica and borosilicate glass, in: IEEE Sensors, Baltimore, MD, USA, 2013, pp. 1767–1770.
[18] D. Senkal, M.J. Ahamed, A.A. Trusov, A.M. Shkel, Demonstration of sub-hz frequency symmetry in micro-glassblown wineglass resonators with integrated electrodes, in: Solid-State Sensors, Actuators and Microsystems Conference (TRANSDUCERS), Barcelona, Spain, 2013, pp. 1380–1383.